Available online at www.sciencedirect.com
ScienceDirect
Trans. Nonferrous Met. Soc. China 23(2013) 2047−2059
Transactions of Nonferrous Metals Society of China
www.tnmsc.cn

Electrochemical hydriding performance of Mg−TM−Mm (TM=transition metals, Mm=mischmetal) alloys for hydrogen storage

V. KNOTEK, D. VOJTĚCH

Department of Metals and Corrosion Engineering, Institute of Chemical Technology, Prague Technická 5, 166 28 Prague 6, Czech Republic

Received 27 July 2012; accepted 5 December 2012

Abstract: Eighteen as-cast binary Mg−Ni, Mg−Mm and ternary Mg−Ni−Mm and Mg−Ni−TM (TM=transition metals (Cu, Zn, Mn and Co); Mm = mischmetal containing Ce, La, Nd and Pr) alloys were hydrided by an electrochemical process to determine the alloys with the most potential for electrochemical hydrogen storage. The alloys were hydrided in a 6 mol/L KOH solution at 80 °C for 480 min and at 100 A/m^2. To assess the electrochemical hydriding performance of alloys, maximum hydrogen concentrations, hydrogen penetration depths and total mass of absorbed hydrogen in the alloys were measured by glow discharge spectrometry. In addition, the structures and phase compositions of the alloys both before and after hydriding were studied by optical and scanning electron microscopy, energy dispersive spectrometry and X-ray diffraction. It was determined that the highest total amount of hydrogen was absorbed by the Mg−25Ni−12Mm and Mg−26Ni (mass fraction, %) alloys. The maximum hydrogen concentrations in the Mg−25Ni−12Mm and Mg−26Ni alloys were 1.0% and 1.6%, respectively. The main hydriding product was the binary MgH_2 hydride, and the ternary Mg_2NiH_4 hydride was also detected in the Mg−25Ni−12Mm alloy. The electrochemical hydriding parameters achieved are discussed in relation to the structures of alloys, alloying elements and hydriding mechanisms.
Key words: hydrogen storage; magnesium; nickel; rare earths; electrochemical hydriding

1 Introduction

Hydrogen is considered to be a potential fuel for future transportation. Additionally, hydrogen is a promising medium for the storage of energy from renewable sources. However, there are technological and safety problems associated with hydrogen storage because hydrogen is an explosive gas and easily penetrates through many materials. For these reasons, hydrogen storage requires expensive pressure and cryogenic containers [1]. A promising alternative is to store hydrogen in the form of metallic hydrides. Hydrides are stable and safe compounds that release hydrogen when heated to sufficient temperatures. Magnesium-based hydrides have been extensively studied because magnesium is light, relatively inexpensive and capable of storing up to 7.6% of hydrogen in the form of MgH_2. However, a well-known drawback of this hydride is its high thermodynamic stability, which is associated with slow hydriding/dehydriding kinetics and high hydrogen release temperature that is above 300°C. For this reason, a large energy input would be needed to obtain hydrogen gas from this storage system. Various efforts have been made to destabilize the MgH_2 phase, which would improve its hydriding/dehydriding behavior. These strategies include the following: 1) the addition of transition metals (TM), such as Ni, Cu, Co, Mn, Zn and rare earths (RE), that form either binary or more complex hydrides including Mg_2NiH_4, Mg_2CoH_5, Mg_3MnH_7, Mg_2RENiH_7 and REH_3 [1−4] and these more complex hydrides usually decompose at lower temperatures than the MgH_2 phase; 2) the addition of catalysts for the hydriding/dehydriding reactions that include RE, transition metal oxides, carbon and halides [5], but the exact catalytic mechanism is not presently known and the mechanism may involve surface modification of magnesium, destruction of the MgO surface layer, enhancement of the formation of atomic hydrogen on the surface or the acceleration of hydrogen diffusion [5]; 3) the preparation of amorphous and/or nano-crystalline structures of the powdered hydride utilizing intensive ball milling, rapid solidification or other techniques. The advantage of ball milling is the

Corresponding author: V. KNOTEK; Tel: +42-22-444055; Fax: +42-220444400; E-mail: Vitezslav.Knotek@vscht.cz
DOI: 10.1016/S1003-6326(13)62695-3

continuous mechanical destruction of the MgH_2 layer, which is a barrier against inward diffusion of hydrogen because H-diffusivity in MgH_2 is significantly slower than that in Mg [5]. Intensive mechanical forces during the milling process also induce high concentrations of lattice defects, grain boundaries and interfaces, which are also good paths for hydrogen diffusion. Rapid solidification techniques, such as melt spinning or gas atomization, provide similar beneficial structural features as those observed in ball milling.

The main barrier associated with the practical use of hydride-based hydrogen storage systems is the high cost of metallic hydrides, which result from the difficult preparation of hydrides. For this reason, the use of hydrides in hydrogen storage is limited. Hydrides are generally produced by elemental synthesis from metal powder and hydrogen gas. In this method, a metallic powder is intensively milled in a hydrogen atmosphere at high temperatures and pressures. Because of the specific properties of hydrogen, elemental synthesis must meet strict requirements in terms of safety, and therefore, this synthetic route is expensive. For this reason, hydrogen storage in pressure and cryogenic containers is presently still preferred over hydrides in technical applications [1].

Recently, we have shown that an alternative to the elemental synthesis of hydrides is electrochemical hydriding [6]. In this process, atomic hydrogen is formed during electrolysis of a suitable aqueous solution on a cathode surface. When the cathode is composed of Mg alloy, hydrogen directly enters the cathode and a hydride phase forms. Hydrided alloys can serve as both portable sources of hydrogen fuel and cathodes for metal hydride based batteries. Electrochemical hydriding is advantageous because it does not require gaseous hydrogen, high temperature or high pressure.

For the above reasons, our study evaluates electrochemical hydriding of various as-cast Mg-based alloys containing transition metals (Ni, Co, Mn, Cu and Zn) and rare earths (RE) that are known to positively affect hydrogen absorption. The structure and electrochemical hydriding efficiency of Mg-based alloys are characterized to identify the material with the most potential for use in hydrogen storage applications. Particular attention is given to the mechanism of electrochemical hydriding, which is potentially different from that of the classical process utilizing hydrogen gas.

2 Experimental

In our work, several binary and ternary Mg−TM−Mm alloys (TM=transition metals Ni, Cu, Zn, Mn or Co; Mm=mischmetal containing 45% Ce, 38% La, 12% Nd and 4% Pr) were hydrided by an electrochemical process as shown in Table 1. Hereafter, all concentrations are in mass fraction. Almost all of the investigated alloys contained nickel as one of the

Table 1 Designations and chemical compositions of studied Mg−TM−Mm alloys

Alloy	*w*/%									
	Ni	Ce	La	Nd	Pr	Mm	Cu	Zn	Co	Mn
Mg−11Ni	10.9	−	−	−	−	−	−	−	−	−
Mg−15Ni	14.8	−	−	−	−	−	−	−	−	−
Mg−26Ni	26.4	−	−	−	−	−	−	−	−	−
Mg−31Ni	31.1	−	−	−	−	−	−	−	−	−
Mg−34Ni	34.2	−	−	−	−	−	−	−	−	−
Mg−52Ni	52.0	−	−	−	−	−	−	−	−	−
Mg−15Mm	−	7.6	3.8	2.7	0.8	14.9	−	−	−	−
Mg−11Ni−6Mm	10.9	3.0	1.6	1.4	0.4	6.4	−	−	−	−
Mg−31Ni−5Mm	31.4	2.5	1.2	1.0	0.3	5.0	−	−	−	−
Mg−24Ni−5Mm	24.0	2.5	1.4	1.1	0.4	5.4	−	−	−	−
Mg−25Ni−9Mm	25.1	4.6	2.2	1.7	0.5	9.0	−	−	−	−
Mg−25Ni−12Mm	25.3	6.0	3.0	2.1	0.6	11.6	−	−	−	−
Mg−26Ni−6Cu	26.5	−	−	−	−	−	6.0	−	−	−
Mg−3Ni−32Cu	2.8	−	−	−	−	−	32.2	−	−	−
Mg−18Ni−23Zn	17.9	−	−	−	−	−	−	22.9	−	−
Mg−26Ni−6Zn	26.1	−	−	−	−	−	−	5.5	−	−
Mg−28Ni−2Mn	27.9	−	−	−	−	−	−	−	−	2.4
Mg−27Ni−5Co	27.5	−	−	−	−	−	−	−	4.9	−

components because nickel increases hydriding kinetics in gaseous hydrogen [7−9]. The first group of alloys consisted of binary Mg−Ni alloys with both hypo- and hyper-eutectic concentrations of Ni (eutectic point in the Mg−Ni diagram corresponds to 23% Ni [10]). These Mg−Ni alloys were used to study the influence of nickel addition on electrochemical hydriding. A binary Mg−Mm alloy was studied to assess the influence of the addition of an individual mischmetal. Another group of alloys consisted of ternary Mg−Ni−Mm alloys in which the concentration of one component was kept almost constant while the concentration of the other component was varied. The purpose of this study was to evaluate the combined role of both additives in the hydriding process because the mischmetal, as a mixture of rare earth elements, is known to accelerate the hydriding/dehydriding kinetics in a similar manner as nickel [11,12]. The last group of investigated alloys contained varying amounts of nickel and other transition metals like Mn, Co, Cu and Zn. Comparing these alloys with binary Mg−Ni alloys, it was possible to estimate the effect of transition metals on electrochemical hydriding. The chemical compositions of the alloys were selected with respect to binary and ternary phase diagrams. The purpose of this study was to prepare alloys in which a significant volume fraction is occupied by disperse eutectic mixtures because relatively rapid hydrogen diffusion can be expected in such alloys even at low temperatures.

The alloys were prepared by vacuum induction melting of pure Mg, TM and Mm (99.9 % purity) under argon. Cylindrical ingots with 200 mm in length and 16 mm in diameter were gravity-cast into a brass mold. Subsequently, the ingots were cut into 0.5-mm-thick pieces for electrochemical hydriding. Prior to hydriding, the surface of the alloys was mechanically polished.

Electrochemical hydriding was conducted in a 6 mol/L KOH solution at 80 °C. The alloys were immersed in an electrolyte, connected to a DC source and polarized as the cathode. A graphite rod with 10 mm in diameter and 100 mm in length was used as the anode. Current density during the hydriding was 100 A/m^2 and hydriding was performed for 480 min. This current density was selected to ensure that a sufficient amount of atomic hydrogen was formed on the cathode surface and to prevent excessive evolution of hydrogen gas.

The structure of as-cast alloys was investigated by light (LM) and scanning electron microscopy (SEM, Tescan Vega 3) and energy dispersion spectrometry (EDS, Oxford Instruments Inca 350). Phase compositions both before and after hydriding were determined by X-ray diffraction (XRD, X′ Pert Pro, Co radiation). To measure the concentration profiles of hydrogen, glow discharge spectrometry (GDS, Profiler 2) was employed. Because hydriding was performed in a strongly alkaline bath, the formation of magnesium hydroxide and/or complex hydroxide surface layers could potentially occur. However, the influence of such layers on the hydrogen profile analysis should be minimal, and only hydrogen present in the metallic phase should be measured. For this reason, the oxygen concentration profile was also analyzed to determine the exact position of the hydroxide/metal interface. The interface was determined to be the point at which the oxygen intensity (concentration) decreases to below the detection limit (see Fig. 1). The GDS analyzer was calibrated using $Mg(OH)_2$ prepared by anodic oxidation of pure Mg. Before calibration, the formation of $Mg(OH)_2$ was verified by XRD. The sputtering rate during depth profiling was calculated from the surface topography measured after analysis by a surface profilometer.

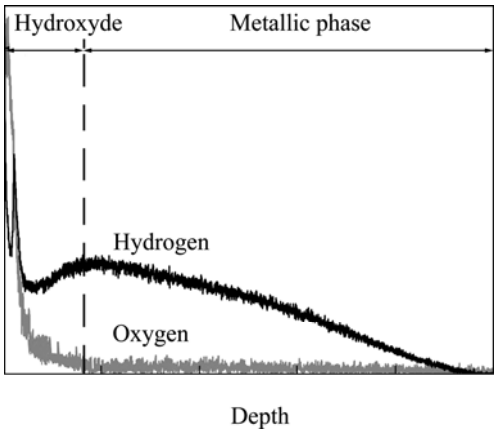

Fig. 1 Analysis of hydrogen concentration profile by GDS (surface hydroxide layer indicated by an increased oxygen concentration was excluded from this analysis. Hydrogen was only measured when it was dissolved in metallic phase)

3 Results

3.1 Structures of alloys

Microstructures of the alloys are presented in Figs. 2−5, and the phase compositions of the alloys determined by XRD and EDS are summarized in Table 2. Figure 2 shows optical micrographs of the binary Mg−Ni and Mg−Mm alloys. The Mg−Ni alloys represent a typical eutectic system [10]. Hypoeutectic alloys, such as Mg−11Ni and Mg−15Ni (Fig. 2(a)), consist of α-Mg dendrites (light) and α-Mg+Mg_2Ni eutectic mixture (dark). The Mg−26Ni alloy is close to the eutectic point (23% Ni), and therefore, its structure is dominated by the α-Mg+Mg_2Ni eutectic mixture (Fig. 2(b)). The Mg−30Ni, Mg−34Ni (Fig. 2(c)) and Mg−52Ni alloys are hypereutectic and contain sharp-edged primary Mg_2Ni

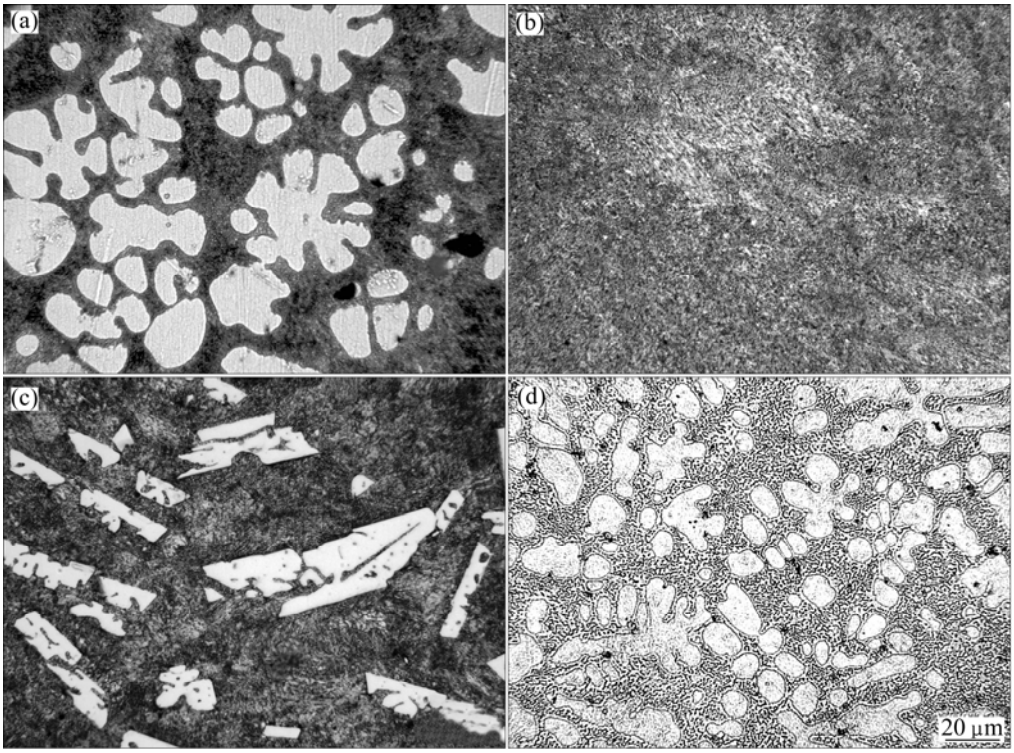

Fig. 2 Optical micrographs of binary alloys: (a) Mg−15Ni (hypoeutectic); (b) Mg−26Ni (almost eutectic); (c) Mg−34Ni (hypereutectic); (d) Mg−15Mm (hypoeutectic)

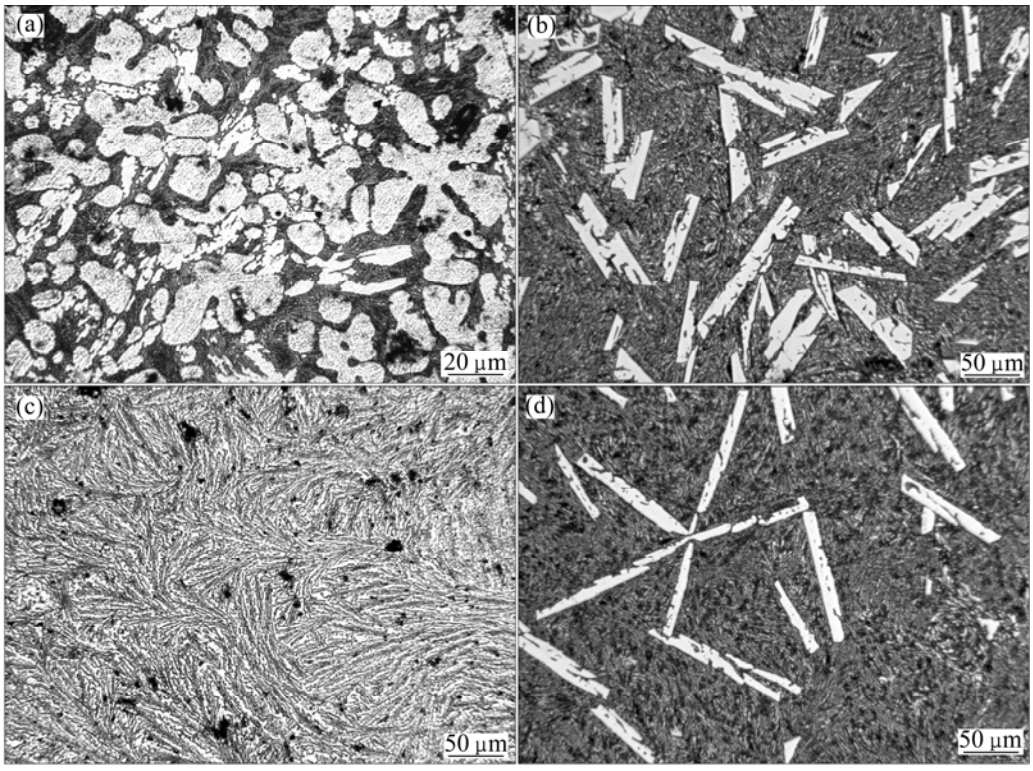

Fig. 3 Optical micrographs of ternary Mg−Ni−Mm alloys: (a) Mg−11Ni−6Mm alloy (hypoeutectic); (b) Mg−31Ni−5Mm alloy (hypereutectic); (c) Mg−24Ni−5Mm alloy (eutectic); (d) Mg−25Ni−12Mm (hypereutectic)

crystals (light) and an α-Mg+Mg_2Ni eutectic mixture (dark). The binary Mg−15Mm alloy also corresponds to a eutectic system, and its structure comprises primary α-Mg dendrites (light) and an α-Mg+$Mg_{12}Mm$ eutectic mixture (Fig. 2(d)). The $Mg_{12}Mm$ phase is a solid solution of isostructural $Mg_{12}Ce$, $Mg_{12}La$, $Mg_{12}Nd$ and $Mg_{12}Pr$ phases (space group $I4/mmm$) [10].

The structural development of ternary Mg−Ni−Mm

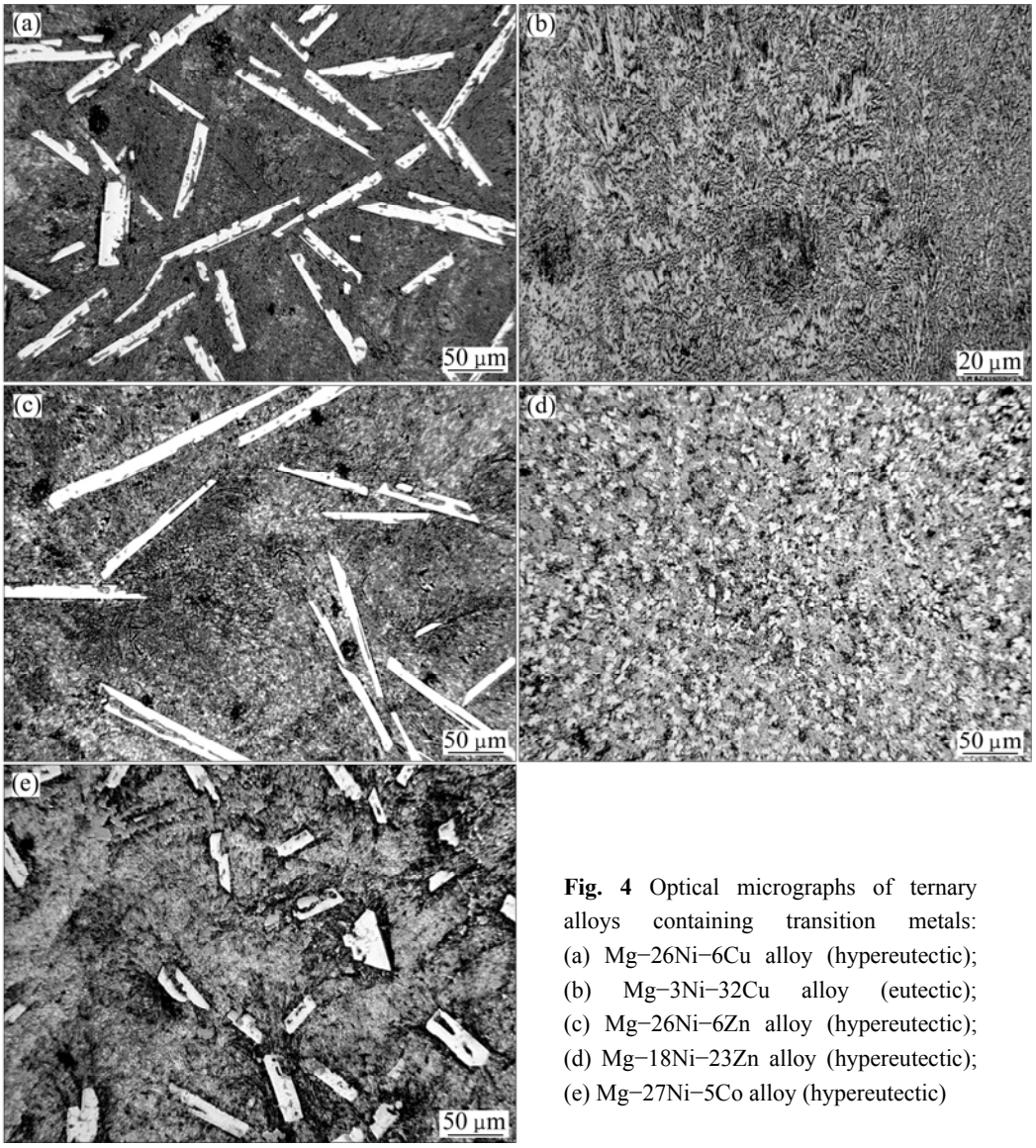

Fig. 4 Optical micrographs of ternary alloys containing transition metals: (a) Mg−26Ni−6Cu alloy (hypereutectic); (b) Mg−3Ni−32Cu alloy (eutectic); (c) Mg−26Ni−6Zn alloy (hypereutectic); (d) Mg−18Ni−23Zn alloy (hypereutectic); (e) Mg−27Ni−5Co alloy (hypereutectic)

Table 2 Phase compositions of investigated Mg−TM−Mm alloys determined by XRD and EDS

Alloy	Phase composition	Alloy	Phase composition
Mg−11Ni	α-Mg, Mg_2Ni	Mg−24Ni−5Mm	α-Mg, Mg_2Ni, $Mg_{12}Mm$
Mg−15Ni	α-Mg, Mg_2Ni	Mg−25Ni−9Mm	α-Mg, Mg_2Ni, $Mg_{12}Mm$
Mg−26Ni	α-Mg, Mg_2Ni	Mg−25Ni−12Mm	α-Mg, Mg_2Ni, $Mg_{12}Mm$
Mg−31Ni	α-Mg, Mg_2Ni	Mg−26Ni−6Cu	α-Mg, Mg_2Ni
Mg−34Ni	α-Mg, Mg_2Ni	Mg−3Ni−32Cu	α-Mg, Mg_2Cu
Mg−52Ni	α-Mg, Mg_2Ni	Mg−18Ni−23Zn	α-Mg, Mg_2Ni, MgZn
Mg−15Mm	α-Mg, $Mg_{12}Mm$	Mg−26Ni−6Zn	α-Mg, Mg_2Ni
Mg−11Ni−6Mm	α-Mg, Mg_2Ni, $Mg_{12}Mm$	Mg−28Ni−2Mn	α-Mg, Mg_2Ni, Mg_3MnNi_2, α-Mn
Mg−31Ni−5Mm	α-Mg, Mg_2Ni, $Mg_{12}Mm$	Mg−27Ni−5Co	α-Mg, Mg_2Ni, $MgCo_2$

alloys with varying Ni and Mm-concentrations is shown in Fig. 3. Table 2 indicates that all of these ternary alloys contain α-Mg, Mg_2Ni and $Mg_{12}Mm$ phases. The Mg−11Ni−6Mm alloy is hypoeutectic (Fig. 3(a)), and it consists of primary α-Mg dendrites (light) and a ternary α-Mg+Mg_2Ni+$Mg_{12}Mm$ eutectic mixture (dark). In contrast, when the nickel concentration of the alloy is 31% (Fig. 3(b)), the structure changes to hypereutectic

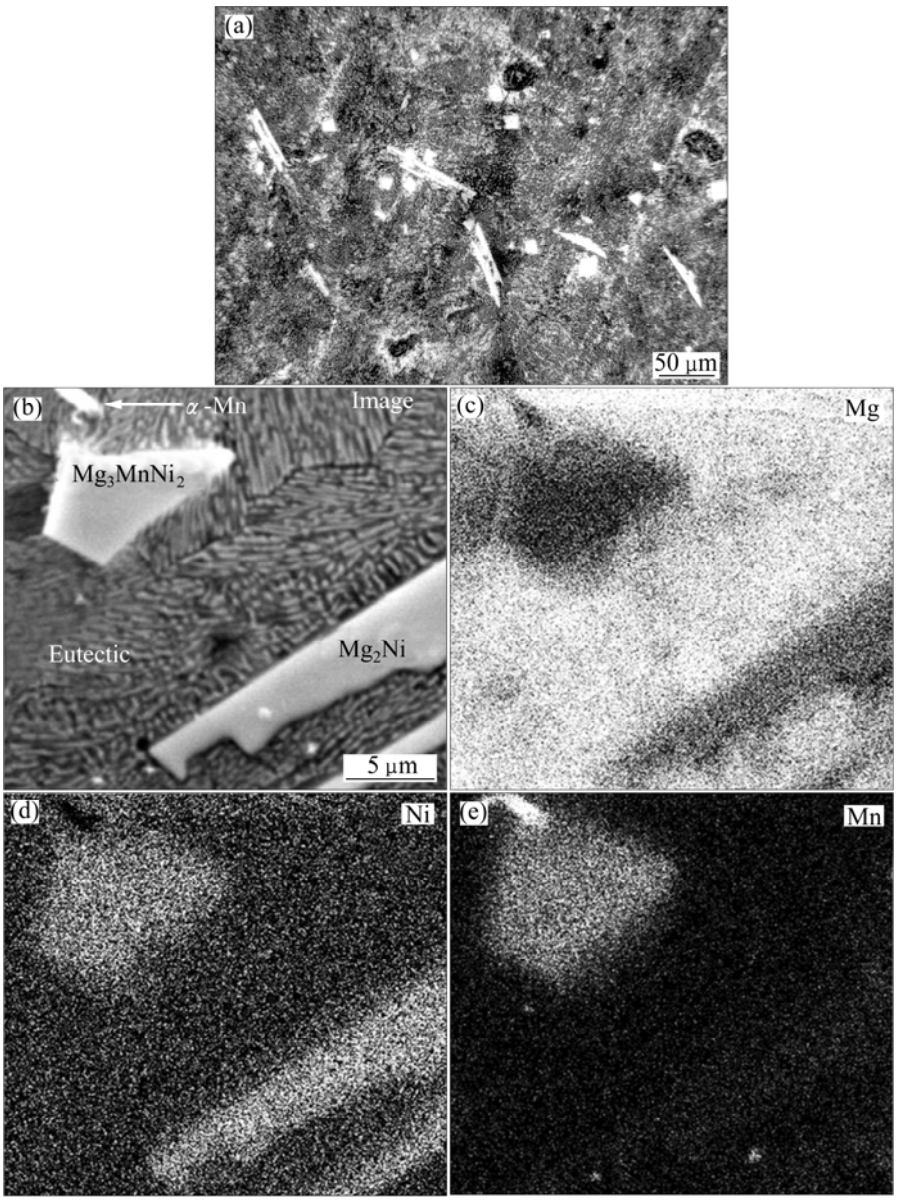

Fig. 5 Structure of Mg−28Ni−2Mn alloy: (a) Optical micrograph; (b) SEM micrograph; (c), (d), (e) X-ray elemental maps

and contains the primary Mg_2Ni phase (light) and the ternary α-Mg+Mg_2Ni+$Mg_{12}Mm$ eutectic (dark). When the concentration of Ni is kept almost constant and the concentration of Mm increases, the structure changes from a ternary eutectic (Mg−24Ni−5Mm alloy, Fig. 3(c)) to a hypereutectic (Mg−25Ni−9Mm and Mg−25Ni−12Mm, Fig. 3(d)). This indicates that the addition of mischmetal shifts the ternary eutectic α-Mg+Mg_2Ni+$Mg_{12}Mm$ to lower nickel concentrations.

Figure 4 shows the structures of the ternary alloys containing Zn, Cu and Co. The Mg−26Ni−6Cu (Fig. 4(a)) is hypereutectic, and it contains primary sharp-edged Mg_2Ni crystals (light) and α-Mg+Mg_2Ni eutectic mixture (dark). EDS analysis indicated that copper is preferentially dissolved in the Mg_2Ni phase. The Mg−3Ni−32Cu approaches the eutectic point of the Mg−Cu system (the eutectic concentration of copper is 31.7% [10]). The structure is therefore almost purely eutectic and is comprised of a α-Mg and a Mg_2Cu phase (Fig. 4(b)). Because of the low nickel concentration, the Mg_2Ni phase is not detected, and thus the nickel remains dissolved in the Mg_2Cu phase. Figure 4(c) illustrates the structure of the Mg−26Ni−6Zn alloy. This structure corresponds to the hypereutectic Mg−Ni alloys and consists of primary Mg_2Ni crystals (light) and α-Mg+Mg_2Ni eutectic (dark). EDS shows that zinc is dissolved in both phases. A different structure is observed for the Mg−18Ni−23Zn alloy (Fig. 4(d)). Both zinc and nickel constitute the ternary eutectic mixture of α-Mg, Mg_2Ni and MgZn phases. In addition, small primary Mg_2Ni

crystals (light) containing dissolved zinc are also present in the structure because the presence of zinc shifts the ternary eutectic point to lower nickel concentrations [13]. A hypereutectic structure also corresponds to the Mg−27Ni−5Co alloy (Fig. 4(e)), which is comprised of primary Mg_2Ni phases (light) and ternary α-Mg+Mg_2Ni+$MgCo_2$ eutectic. Despite the low Mn concentration of the Mg−28Ni−2Mn alloy, the structure of this alloy is complicated and is thus present separately in Fig. 5. An optical micrograph in Fig. 5(a) indicates that there are at least two types of sharp-edged primary crystals (light), one of which is elongated and the other has an almost equi-axed shape. There is also a dispersed α-Mg + Mg_2Ni eutectic mixture (dark). A more detailed SEM image and X-ray elemental maps in Fig. 5 show that the elongated crystals correspond to Mg_2Ni phase and that the equi-axed crystals correspond to ternary Mg_3MnNi_2 phase [14]. The elemental maps also detect the presence of small particles of pure α-Mn.

3.2 Hydrogen concentration profiles

Hydrogen concentration profiles are shown in Fig. 6. Table 3 summarizes hydriding parameters obtained from these profiles including the maximum hydrogen concentrations present on the alloy surface, the hydrogen penetration depths and the total mass of hydrogen absorbed in the alloys during hydriding. Values of the last parameter in Table 3 are seemingly small, but it should be taken into account because hydrided volumes are very small.

The influence of nickel on the electrochemical hydriding behavior is illustrated in Fig. 6(a). The maximum values of the hydriding parameters are obtained for the Mg−26Ni alloy, the structure of which is eutectic (Fig. 2(b)). When either primary α-Mg or primary Mg_2Ni form in the structure (Fig. 2), all the hydriding parameters decrease. A similar trend is observed when the hypoeutectic Mg−11Ni−6Mm, the eutectic Mg−24Ni−5Mm and the hypereutectic Mg−31Ni−5Mm alloys with similar concentration of Mm are compared in Table 3. The eutectic alloys again exhibit the highest hydriding parameters. This behavior differs from the classical hydriding processes performed by milling of alloys in hydrogen gas. In classical processes, hydriding efficiency commonly increases with increasing Ni content because of the formation of the ternary Mg_2NiH_4 hydride [7,8]. Microstructural characteristics of the as-cast alloys play a significant role in the electrochemical hydriding process. When nickel is absent in the alloy (Mg−15Mm), electrochemical hydriding is not very efficient, and a penetration depth of only 12 μm is achieved (Table 3).

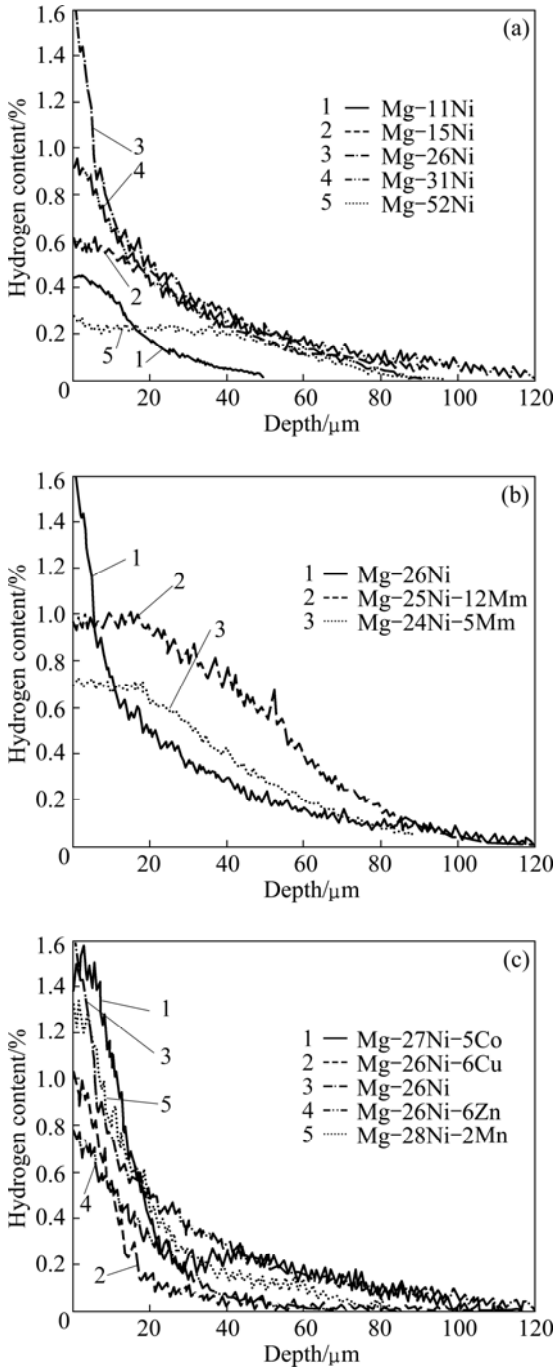

Fig. 6 Hydrogen concentration profiles after electrochemical hydriding: (a) Mg−Ni alloys; (b) Mg−Ni−Mm alloys; (c) Ternary Mg−Ni−TM (TM=Co, Cu, Mn, Zn) alloys

Figure 6(b) illustrates the influence of mischmetal addition on the hydriding parameters of alloys in which the Ni concentration is kept almost constant. In the Mm-free Mg−26Ni alloy, a maximum of 1.6% of hydrogen is reached on the surface, and H-concentration decreases steeply beneath the surface. In contrast, on the Mm-containing alloys, the maximum concentrations of hydrogen are lower (between 0.7 and 1.0). However, the decrease rate of concentration is significantly slower towards the alloy interior. Additionally, the total mass of

hydrogen absorbed in the Mg−26Ni−12Mm alloy is significantly higher than that of the eutectic binary alloy. When the amount of absorbed hydrogen was considered, the Mg−26Ni− 12Mm alloy exhibited the best hydriding efficiency among all the investigated alloys (Table 3).

Table 3 Hydriding parameters including maximum hydrogen concentrations on alloy surface ($w_{max.}$), hydrogen penetration depths (X) and total mass (m) of hydrogen absorbed in alloys after electrochemical hydriding

Alloy	w_{max}/%	X/μm	m/μg
Mg−11Ni	0.4	50	34
Mg−15Ni	0.6	90	74
Mg−26Ni	1.6	120	170
Mg−31Ni	1.0	110	150
Mg−34Ni	0.9	90	124
Mg−52Ni	0.3	90	89
Mg−15Mm	0.6	12	13
Mg−11Ni−6Mm	0.6	60	85
Mg−31Ni−5Mm	0.5	80	134
Mg−24Ni−5Mm	0.7	90	156
Mg−25Ni−9Mm	0.8	80	148
Mg−25Ni−12Mm	1.0	120	280
Mg−26Ni−6Cu	1.0	60	60
Mg−3Ni−32Cu	1.4	30	71
Mg−18Ni−23Zn	0.8	70	79
Mg−26Ni−6Zn	0.8	60	75
Mg−28Ni−2Mn	1.3	80	120
Mg−27Ni−5Co	1.6	100	158

The influence of low Cu, Co, Zn and Mn additions on the hydriding behavior is illustrated in Fig. 6(c). The data shown in this figure and the hydriding parameters in Table 3 indicate that Cu, Mn and Zn negatively influence the electrochemical hydriding performance. The Mg−26Ni−6Cu, Mg−26Ni−6Zn and Mg−28Ni−2Mn alloys have lower hydriding parameters than the simple binary Mg−26Ni alloy, although the influence of Mn is relatively weak. When the concentrations of Zn and Cu are significantly increased at the expense of Ni (Mg−18Ni−23Zn and Mg−3Ni−32Cu alloys), the total mass of absorbed hydrogen remains similar to those of the Mg−26Ni−6Zn and Mg−26Ni−6Cu alloys (Table 3). This similarity suggests that both Cu and Zn do not significantly affect the hydriding performance and that the observed decrease of the hydriding parameters in comparison with the binary Mg−26Ni alloy is because of the reduction of the volume fraction of the disperse α-Mg+Mg_2Ni eutectic mixture (Figs. 2(b), 4(a) and 4(c)). A similar rationale can explain the slight negative effect of manganese addition. In contrast to Cu, Zn and Mn, the addition of Co has no significant effect on hydriding parameters (Table 3), despite the observed decrease in the volume fraction of the disperse eutectic (Figs. 2(b) and 4(e)). This result suggests that the hydriding mechanism of the Co-containing alloy is different from that of the binary Mg−26Ni alloy.

3.3 Phase composition after hydriding

To assess the mechanism of electrochemical hydriding, the hydrided alloys were analyzed by XRD. Because electrochemical hydriding affected relatively thin surface layers in the order of several tens of micron, the identification of hydrides was difficult. The characteristic peaks of hydrides were significantly masked by peaks associated with the dominating phases of the structure. Therefore, it was possible to detect only major hydride phases. Additionally, no hydrides were detected in the alloys that had absorbed small amounts of hydrogen because of the limited sensitivity of XRD. XRD patterns of the hydrided Mg−26Ni and Mg−25Ni−12Mm alloys that absorbed the largest mass of hydrogen are illustrated in Fig. 7, and the results of XRD measurements are summarized in Table 4.

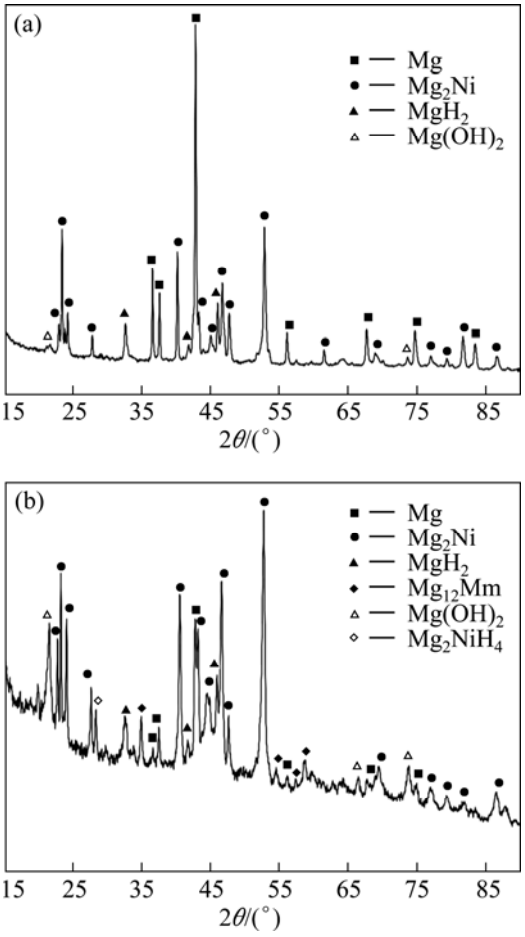

Fig. 7 XRD patterns of hydrided Mg−26Ni (a) and Mg−26Ni−12Mm alloys (b)

Figure 7 demonstrates that the XRD patterns of these materials are relatively complicated and contain a number of characteristic peaks. By careful analysis of the pattern corresponding to the hydrided binary Mg−26Ni alloy, it was determined that the main hydriding product of this alloy is the MgH_2 binary hydride. The largest peak in the diffraction pattern of this hydride is found at a diffraction angle of 32.5°. The MgH_2 hydride is also detected in the other hydrided alloy, but the XRD pattern of this alloy also indicates the presence of the ternary low temperature (LT) monoclinic Mg_2NiH_4 hydride. Mg_2NiH_4 hydride has a characteristic peak located at 2θ=28°. The other significant peaks of this phase are masked by peaks associated with the phases that compose the base alloy. The list of hydriding products in Table 4 implies that the ternary hydride forms only in two alloys during hydriding, namely in the Mg−25Ni−12Mm alloy and potentially in the Mg−27Ni−5Co alloy. In the other hydrided materials, only the simple MgH_2 hydride was detected and the volume fractions of the ternary Mg_2NiH_4 hydride or other hydrides were below the XRD detection limit.

Table 4 Hydride phases present in investigated alloys after electrochemical hydriding

Alloy	Present hydride
Mg−11Ni	−
Mg−15Ni	MgH_2
Mg−26Ni	MgH_2
Mg−31Ni	MgH_2
Mg−34Ni	MgH_2
Mg−52Ni	−
Mg−15Mm	−
Mg−11Ni−6Mm	−
Mg−31Ni−5Mm	MgH_2
Mg−24Ni−5Mm	MgH_2
Mg−25Ni−9Mm	MgH_2
Mg−25Ni−12Mm	MgH_2, Mg_2NiH_4
Mg−26Ni−6Cu	MgH_2
Mg−3Ni−32Cu	MgH_2
Mg−18Ni−23Zn	MgH_2
Mg−26Ni−6Zn	MgH_2
Mg−28Ni−2Mn	MgH_2
Mg−27Ni−5Co	MgH_2, (Mg_2NiH_4)*

* The presence of this phase is uncertain

4 Discussion

4.1 Electrochemical hydriding mechanism

The first stage of electrochemical hydriding is the formation of atomic hydrogen on the cathode surface through an electrochemical reaction:

$$H_2O+e^- \rightarrow H+OH^- \quad (1)$$

Atomic hydrogen then diffuses into the cathode material both along phase boundaries and through the phases present in the structure. It was shown in our previous paper [15] that electrochemical hydriding does not work for pure Mg, which is potentially because of a negligible solubility of hydrogen in solid magnesium that results in the rapid formation of a surface MgH_2 layer. The formation of this layer prevents hydrogen from further inward diffusion. The diffusion coefficient of H in MgH_2 is significantly lower than in Mg [5]. To support the inward diffusion of hydrogen, the presence of an appropriate alloying element is necessary, of which nickel is the most important. It forms a disperse eutectic that is composed of α-Mg and Mg_2Ni phases. In this alloy, hydrogen diffuses both along the interphase boundaries and in the Mg_2Ni phase to form the interstitial solid solution $Mg_2NiH_{0.3}$:

$$Mg_2Ni+0.3H \rightarrow Mg_2NiH_{0.3} \quad (2)$$

Both Mg_2Ni and $Mg_2NiH_{0.3}$ have hexagonal crystal lattices (space group $P6_222$). Therefore, these phases are difficult to distinguish using XRD. Finally, hydrogen that is diffusing in the eutectic regions preferentially reacts with Mg to form MgH_2 as the main hydriding product of the alloy (Table 4).

$$Mg+2H \rightarrow MgH_2 \quad (3)$$

Through this mechanism, hydrogen is able to penetrate relatively deeply into the material. Additionally, the formation of MgH_2 is significantly more advantageous than other types of hydrides because of the hydrogen gravimetric density and energy storage density. Figure 7 and Table 4 indicate that a competitive hydriding reaction should be considered in the Mg−25Ni−12Mm and Mg−27Ni−5Co alloys, which produces the ternary Mg_2NiH_4 hydride:

$$Mg_2NiH_{0.3}+3.7H \rightarrow Mg_2NiH_4 \quad (4)$$

4.2 Influence of alloying elements on electrochemical hydriding performance

4.2.1 Nickel

Nickel has been known for many years to support hydriding in hydrogen gas [7−9]. Nickel catalyzes the dissociation of molecular hydrogen to atomic hydrogen on the surface. Atomic hydrogen is then capable of diffusing into the metallic phase. A similar mechanism can be expected in the case of electrochemical hydriding where nickel catalyzes the electrochemical reaction depicted in Eq. (1). Nickel also readily forms the ternary

Mg_2NiH_4 hydride during hydriding in hydrogen gas at elevated temperatures. The positive influence of nickel is generally attributed to its electronic structure that includes d-bands containing unpaired valence electrons. The interaction of the unpaired d-electrons of nickel with the 1s-electron of atomic hydrogen leads to the coupling of valence electrons and to a reduction of energy. Therefore, nickel stabilizes atomic hydrogen.

In a number of papers, it has been shown that the hydriding performance in hydrogen gas is proportional to nickel content [7,8]. However, in our experiment this proportionality is not valid for the electrochemical hydriding of cast alloys. Among the binary Mg−Ni alloys investigated, the best hydriding performance is observed for the eutectic Mg−26Ni alloy (Fig. 6(a) and Table 3). The disperse eutectic structure (Fig. 2(b)) with a high volume fraction of interphase boundaries most likely provides a good path for the inward diffusion of hydrogen. In addition, in this type of structure there is a large $Mg_2NiH_{0.3}$/α-Mg interphase area, where the α-Mg phase reacts with hydrogen. When the volume fraction of the eutectic mixture decreases (hypo- and hyper-eutectic alloys, Fig. 2), the rate of hydrogen diffusion and the reaction area decrease.

Hydrogen diffusing in the eutectic structure reacts with α-Mg phase to form the main hydriding product, MgH_2 (Eq. (3)). It is known that this hydride is a barrier for further hydrogen diffusion into α-Mg, and therefore, hydrogen concentration rapidly decreases towards the alloy interior (Fig. 6(a)). However, it can be assumed that large hydrogen gravimetric densities can be reached by refining the structure through techniques such as rapid solidification or milling. XRD analysis reveals that the formation of the ternary LT Mg_2NiH_4 hydride (Eq. (4)) is not significant during electrochemical hydriding of the binary Mg−Ni alloys (Table 4). The original $Mg_2NiH_{0.3}$ phase is characterized by the $P6_222$ space group with lattice parameters a=0.525 nm and c=1.343 nm [16]. The low temperature Mg_2NiH_4 hydride has the $C2/c$ space group with parameters a=1.434 nm, b=0.640 nm and c=0.648 nm [9]. Therefore, the transformation of the former crystal structure to the latter would require a large lattice expansion and beveling. The absence of the ternary hydride may be a result of the high activation energy needed for this atomic rearrangement. At the low temperatures used in electrochemical hydriding, thermal vibrations are not sufficient to overcome this energy barrier. Alternatively, the MgH_2 hydride has a tetragonal lattice (the $P42/mnm$ space group) with unit cell parameters a=0.452 nm and c=0.302 nm [16]. Comparing these parameters with those of α-Mg (hexagonal $P63/mmc$ space group with parameters a=0.324 nm and c=0.526 nm [16]), it can be assumed that the transformation depicted by Eq. (3) proceeds more readily and faster than that given by Eq. (4) [14,16,17].

4.2.2 Mischmetal

Mischmetal is a mixture of REs (in our case Ce, La, Nd and Pr) and has a positive effect on the electrochemical hydriding of magnesium. This effect can be observed by comparing the Mg−15Mm alloy (Table 3) and pure Mg, which is able to absorb only a negligible amount of hydrogen during the electrochemical process because of the rapid formation of MgH_2 that acts as a barrier against further hydriding [15]. Similar behavior is observed during hydriding in hydrogen gas. It is believed that REs catalyze the formation of atomic hydrogen, and similar to nickel, the interactions of the unoccupied f-orbitals and unpaired d- and f-electrons in the RE's valence bands with the unpaired s-electrons of hydrogen may account for this effect [18]. Additionally, REs can form special hydrides including Mg_2RENiH_7, Mg_3REH_9 and REH_2 [3,4,11]. Despite a similarity between REs and Ni, the effect of mischmetal appears to be weaker, which is evident from a comparison of the hydriding parameters of the Mg−Mm and Mg−Ni alloys in Table 3. Concretely, the binary Mg−15Ni alloy absorbed nearly six times higher amount of hydrogen than the binary Mg−15Mm alloy. Therefore, binary Mg−Mm alloys are probably not suitable for electrochemical hydriding.

As shown in Table 3, the ternary Mg−Ni−Mm alloys show interesting hydriding behavior. At Mm-concentrations of approximately 5%−6% (the Mg−11Ni−6Mm, Mg−24Ni−5Mm and Mg−31Ni−5Mm alloys), the hydriding behavior primarily depends on the volume fraction of the disperse eutectic (Fig. 3). Increasing the fraction of disperse eutectic results in an increase in the hydriding performance. One exception is the Mg−25Ni−12Mm alloy whose structure is hypereutectic (Fig. 3(d)), and it contains a lower volume fraction of eutectic mixture than the Mg−26Ni or Mg−24Ni−5Mm alloys. Despite these structural features, the Mg−25Ni−12Mm alloy has the best hydriding performance in terms of the total mass of absorbed hydrogen (Table 3). Figure 6(b) also shows that hydrogen diffusion proceeds faster in this alloy than in the binary Mg−26Ni alloy because the hydrogen concentration gradient is smaller. One explanation for this difference is the potential formation of the ternary Mg_2NiH_4 hydride in the Mg−25Ni−12Mm alloy (Fig. 7 and Table 4). The diffusion coefficient of hydrogen in the ternary hydride is higher than the coefficient in the binary MgH_2 phase because Ni—H bonds are weaker

than Mg—H bonds [5]. Therefore, once the ternary hydride partially replaces MgH_2 during hydriding of the Mg−25Ni−12Mm alloy, the barrier for inward hydrogen diffusion decreases. The other Mg−Ni−Mm alloys in Fig. 6(b) also exhibit low H-concentration gradients, but the ternary hydride is not detected in these alloy, probably because of the difficulties inherent to XRD analysis described above. The observed promotion of Mg_2NiH_4 hydride formation by mischmetal is an important finding that requires more detailed investigation. Potentially, large RE atoms incorporate into the eutectic $Mg_2NiH_{0.3}$ phase, which induces internal stress and reduces the stability of this phase. The $Mg_2NiH_{0.3}$ phase then becomes more likely to be transformed to Mg_2NiH_4 (Eq. (4)).

In terms of hydrogen storage density, a combination of two hydriding products, namely MgH_2 and Mg_2NiH_4, appears to be beneficial because the former increases the maximum hydrogen concentration, while the latter facilitates hydrogen diffusion.

4.2.3 Copper and zinc

Figure 6(c) and Table 3 indicate that both of these elements influence the electrochemical hydriding performance negatively because these elements decrease the volume fraction of the disperse Mg_2Ni+α-Mg eutectic (Fig. 4). Although the Mg−3Ni−32Cu alloy has a purely eutectic structure (Fig. 4(b)) in which fast hydrogen diffusion could be expected because this alloy also has low hydriding parameters (Table 3). A negligible catalytic effect of Cu and Zn on electrochemical hydriding can be explained by evaluating the electron structure of these elements. Both elements have d-valence orbitals that are fully occupied by paired electrons. Zn also has a fully occupied s-orbital, and in Cu, there is one unpaired s-electron. Therefore, an interaction of these electrons with the 1s-electron of hydrogen would lead to the antibonding coupling of electrons. Antibonding coupling always increases the energy of a system, and it is a repulsive bonding contribution [18]. For this reason, Zn−H and Cu−H interactions do not play a role in electrochemical hydriding.

4.2.4 Manganese

Manganese is described separately from copper and zinc because of its different valence electron structure. The electron configuration of Mn is $3d^5 4s^2$. Therefore, there is a large potential for the coupling of the five unpaired d-electrons with the s-electron of hydrogen, and an increased hydriding activity of Mn-containing alloys could be expected. It has been reported recently that Mg−Ni−Mn alloys are prospective materials for hydriding in hydrogen gas because of the catalytic properties of the Mg_3MnNi_2 phase present in the material [14]. VEGGE et al [18] confirmed the possible catalytic effect of Mn by calculating hydride formation energies and the TM−H chemical bond energies of various TMs by density functional theory. They found that the most negative energies of both hydride formation and chemical bonds corresponded to those TMs whose d-bands contain five or slightly more than five valence electrons such as Mn, Fe and Co. In the as-cast Mg−28Ni−2Mn alloy studied in this work, the Mg_3MnNi_2 phase is also present, but its volume fraction is low (Fig. 5). Therefore, the possible catalytic effect of this phase on electrochemical hydriding is probably negated by the observed decrease in the volume fraction of α-Mg+Mg_2Ni eutectic mixture because of both the addition of Mn and the slightly increased concentration of Ni. Therefore, the hydriding parameters of the Mg−28Ni−2Mn alloy are slightly lower than those of the binary Mg−26Ni alloy (Fig. 6 and Table 3).

4.2.5 Cobalt

By comparing the hydriding parameters of the Mg−27Ni−5Co and Mg−26Ni alloys, one can observe that the addition of Co has a small effect on the hydriding parameters (Table 3). Cobalt only slightly reduces the total mass of hydrogen and the penetration depth of hydrogen. However, Fig. 4(e) indicates that cobalt supports the formation of Mg_2Ni primary crystals because cobalt reduces the volume fraction of the eutectic, similarly to Zn (Fig. 4(c)) and Cu (Fig. 4(a)). As described previously, the negative effect of such a structural modification may be balanced by the catalytic effect of Co that results from its electron structure [18]. A positive influence of Co on hydriding performed in hydrogen gas was also reported in Ref. [19]. Additionally, XRD analysis performed after hydriding of the Mg−27Ni−5Co alloy (Table 4) indicated the presence of a small amount of the ternary Mg_2NiH_4 hydride. Hydrogen diffusion proceeds faster in this ternary hydride than in the binary MgH_2 phase [5].

5 Conclusions

Based on the obtained results, it can be concluded that the electrochemical hydriding performance of as-cast Mg-based alloys strongly depends on both the alloying elements and the structural states present. Hydriding is supported by the presence of both a fine eutectic structure composed of α-Mg and an intermetallic phase rich in elements having a catalytic effect on hydriding (Ni, Co and RE). In terms of hydrogen surface concentration and hydrogen penetration depth, the best hydriding performance is

observed for the Mg−26Ni alloy with a purely eutectic structure. However, regarding the total mass of hydrogen absorbed during electrochemical hydriding, the Mg−25Ni−12Mm alloy has the best performance. In this alloy, catalytic activities of both Ni and Mm are combined, and the Mm addition also changes the hydriding mechanism and facilitates the inward diffusion of hydrogen. Both the Mg−26Ni and Mg−25Ni−12Mm alloys are prospective materials for electrochemical storage of hydrogen because the main hydriding product of these alloys is the binary MgH_2 hydride that can theoretically absorb 7.6% of hydrogen. The maximum hydrogen concentrations of 1.6% and 1% reached in this study are seemingly low, but it should be taken into account that the studied alloys were in the as-cast state. Despite the presence of disperse eutectic mixtures in the as-cast alloys, there are many potential options to further refine the structure and to significantly increase the electrochemical hydriding performance of the alloys by, for example, using mechanical milling and/or rapid solidification techniques. The main objective of this study was to identify the alloys with the most potential for electrochemical hydrogen storage. Further studies will be devoted to designing suitable cathodes of these alloys that are capable of storing high amounts of hydrogen and energy.

Acknowledgements

Research on the electrochemical preparation of hydrides is financially supported by the Czech Science Foundation (project no. P108/12/G043).

References

[1] ROSS D K. Hydrogen storage: The major technological barrier to the development of hydrogen fuel cell cars [J]. Vacuum, 2006, 80: 1084−1089.

[2] WU Y, LOTOTSKY M V, SOLBERG J K, YARTYS V A, HAN W, ZHOU S X. Microstructure and novel hydrogen storage properties of melt-spun Mg−Ni−Mm alloys [J]. Journal of Alloys and Compounds, 2009, 477(1): 262−266.

[3] OUYANG L Z, YANG X S, DONG H W, ZHU M. Structure and hydrogen storage properties of Mg_3Pr and $Mg_3PrNi_{0.1}$ alloys [J]. Scripta Materialia, 2009, 61(4): 339−342.

[4] OUYANG L Z, DONG H W, ZHU M. Mg_3Mm compound based hydrogen storage materials [J]. Journal of Alloys and Compounds, 2007, 446−447: 124−128.

[5] JAIN I P, LAL C, JAIN A. Hydrogen storage in Mg: A most promising material [J]. International Journal of Hydrogen Energy, 2010, 35(10): 5133−5144.

[6] VOJTĚCH D, ŠUŠTARŠIČ B, MORŤANIKOVÁ M, MICHALCOVÁ A, VESELÁ A. Electrochemical hydriding as method for hydrogen storage? [J]. International Journal of Hydrogen Energy, 2009, 34(17): 7239−7245.

[7] SONG M Y. Effects of mechanical alloying on the hydrogen storage characteristics of Mg-$x$wt%Ni (x=0, 5, 10, 25 and 55) mixtures [J]. International Journal of Hydrogen Energy, 1995, 20(3): 221−227.

[8] BERLOUIS L E A, CABRERA E, HALL-BARIENTOS E, HALL P J, DODD S, MORRIS S, IMAM M A. A thermal analysis investigation of the hydriding properties of nanocrystalline Mg−Ni based alloys prepared by high energy ball milling [J]. Journal of Alloys and Compounds, 2000, 305(1−2): 82−89.

[9] ZHANG J, ZHOU D W, HE L P, PENG P, LIU J S. First-principles investigation of Mg_2Ni phase and high/low temperature Mg_2NiH_4 complex hydrides [J]. Journal of Physics and Chemistry of Solids, 2009, 70(1): 32−39.

[10] GALE W F, TOTEMEIER T C. Smithells metals reference book [M]. Amsterdam: Elsevier Publishers, 2004.

[11] LØKEN S, SOLBERG J K, MAEHLEN J P, DENYS R V, LOTOTSKY M V, TARASOV B P, YARTYS V A. Nanostructured Mg–Mm–Ni hydrogen storage alloy: Structure — properties relationship [J]. Journal of Alloys and Compounds, 2007, 446−447: 114−120.

[12] WU Y, HAN W, ZHOU S X, LOTOTSKY M V, SOLBERG J K, YARTYS V A. Microstructure and hydrogenation behavior of ball-milled and melt-spun Mg−10Ni−2Mm alloys [J]. Journal of Alloys and Compounds, 2008, 466(1−2): 176−181.

[13] BHAN S, JAIN K C, LAL A. The Mg−Ni−Zn system (magnesium−nickel−zinc) [J]. Journal of Phase Equilibria, 1997, 18: 305−310.

[14] DENYS R V, ZAVALIY I Y, BONCOUR V P, BEREZOVETS V V, KOVALCHUK I V, RIABOV A B. New Mg−Mn−Ni alloys as efficient hydrogen storage materials [J]. Intermetallics, 2010, 18(8): 1579−1585.

[15] VOJTĚCH D, GUHLOVÁ P, MORŤANIKOVÁ M, JANÍK P. Hydrogen storage by direct electrochemical hydriding of Mg-based alloys [J]. Journal of Alloys and Compounds, 2010, 494(1−2): 456−462.

[16] DENYS R V, RIABOV A B, MAEHLEN J P, LOTOTSKY M V, SOLBERG J K, YARTYS V A. In situ synchrotron X-ray diffraction studies of hydrogen desorption and absorption properties of Mg and Mg−Mm−Ni after reactive ball milling in hydrogen [J]. Acta Materialia, 2009, 57(13): 3989−4000.

[17] KALISVAART W P, HARROWER C T, HAAGSMA J, ZAHIRI B, LUBER E J, OPHUS C, POIRIER E, FRITYSCHE H, MITLIN D. Hydrogen storage in binary and ternary mg-based alloys: A comprehensive experimental study [J]. International Journal of Hydrogen Energy, 2010, 35(5): 2091−2103.

[18] VEGGE T, HEDEGAARD-JENSEN L S, BONDE J, MUNTER T R, NORSKOV J K. Trends in hydride formation energies for magnesium-3d transition metal alloys [J]. Journal of Alloys and Compounds, 2005, 386(1−2): 1−7.

[19] ZHANG Yang-huan, REN Hui-ping, LI Bao-wei, GUO Shi-hai, PANG Zai-guang, WANG Xin-lin. Electrochemical hydrogen storage characteristics of nanocrystalline and amorphous $Mg_{20}Ni_{10-x}Co_x$ (X= 0−4) alloys prepared by melt spinning [J]. International Journal of Hydrogen Energy, 2009, 34(19): 8144−8151.

Mg−TM−Mm (TM=过渡金属，Mm=混合稀土) 贮储氢合金的电化学性能

V. KNOTEK, D. VOJTĚCH

Department of Metals and Corrosion Engineering, Institute of Chemical Technology, Prague Technická 5, 166 28 Prague 6, Czech Republic

摘　要：对 18 种铸造态合金，包括二元合金 Mg−Ni、Mg−Mm 和三元合金 Mg−Ni−Mm、Mg−Ni−TM(TM=过渡金属(Cu，Zn，Mn 和 Co)；Mn=含 Ce，La，Nd 和 Pr 的混合稀土)，采用电化学方法进行氢化，选取最具有潜力的电化学贮氢材料。将这些合金在 80 °C 的 6 mol/L KOH 溶液中以电流密度 100 A/m^2 氢化 480 min。为了评价合金的电化学氢化性能，采用辉光放电光谱法测定氢化后合金的最大氢气浓度、氢渗透深度、总的吸氢质量。采用光学和扫描电子显微镜、能谱和X射线衍射测试分析合金的结构与相组成。结果表明，Mg−25Ni−12Mm 和 Mg−26Ni 合金具有最大的吸氢质量，其吸附的最大的氢浓度分别为 1.0%和 1.6%；主要的氢化产品为二元氢化物 MgH_2，在 Mg−25Ni−12Mm 合金中也检测到有三元氢化物 Mg_2NiH_4。讨论了电化学氢化参数对合金的结构、合金化元素和氢化机理的影响。

关键词：贮氢；镁；镍；稀土；电化学氢化

(Edited by Hua YANG)